Eur. Phys. J. C (2014) 74:2763
DOI 10.1140/epjc/s10052-014-2763-0

THE EUROPEAN PHYSICAL JOURNAL C

Regular Article - Theoretical Physics

Positivity constraints on the low-energy constants of the chiral pion–nucleon Lagrangian

Juan José Sanz-Cillero[1,a], **De-Liang Yao**[2,b], **Han-Qing Zheng**[3,4,c]

[1] Departamento de Física Teórica and Instituto de Física Teórica, IFT-UAM/CSIC Universidad Autónoma de Madrid , Cantoblanco, Madrid, Spain
[2] Institute for Advanced Simulation, Institut für Kernphysik and Jülich Center for Hadron Physics, Forschungszentrum Jülich, 52425 Jülich, Germany
[3] Department of Physics and State Key Laboratory of Nuclear Physics and Technology, Peking University, Beijing 100871, People's Republic of China
[4] Collaborative Innovation Center of Quantum Matter, Beijing, People's Republic of China

Received: 16 December 2013 / Accepted: 29 January 2014 / Published online: 5 March 2014

Abstract Positivity constraints on the pion–nucleon scattering amplitude are derived in this article with the help of general S-matrix arguments, such as analyticity, crossing symmetry, and unitarity, in the upper part of the Mandelstam triangle, $\mathcal{R}$. Scanning inside the region $\mathcal{R}$, the most stringent bounds on the chiral low-energy constants of the pion–nucleon Lagrangian are determined. When just considering the central values of the fit results from covariant baryon chiral perturbation theory using the extended-on-mass-shell scheme, it is found that these bounds are well respected numerically both at the $O(p^3)$ and the $O(p^4)$ level. Nevertheless, when taking the errors into account, only the $O(p^4)$ bounds are obeyed in the full error interval, while the bounds on the $O(p^3)$ fits are slightly violated. If one disregards the loop contributions, the bounds always fail in certain regions of $\mathcal{R}$. Thus, at a given chiral order these terms are not numerically negligible and one needs to consider all possible contributions, i.e., both tree-level and loop diagrams.We have provided the constraints for special points in $\mathcal{R}$ where the bounds are nearly optimal in terms of just a few chiral couplings, which can easily be implemented and employed to constrain future analyses. Some issues concerned with calculations with an explicit Δ resonance are also discussed.

1 Introduction

Chiral perturbation theory (χPT) [1–3] plays an important role in studying low-energy hadron physics, such as the pion–nucleon interaction. Many efforts have been made to study pion–nucleon physics [4,5] within baryon chiral perturbation theory (BχPT) [6,7] using different approaches, e.g., heavy baryon (HB) χPT [8,9], infrared regularization (IR) [10,11], extended on mass shell (EOMS) [12,13], etc. The scattering amplitudes are then expressed in terms of the low-energy constants (LECs). As is well known, when stepping up to higher and higher orders, there always appear a rapidly growing number of LECs, which are free parameters, not fixed by chiral symmetry. Nevertheless, general S-matrix arguments such as analyticity, crossing, and unitarity can be used to constrain the pion–nucleon interaction and its chiral effective theory description. It is therefore possible to obtain certain model-independent constraints on the LECs.

Along this line, many works have been devoted to the study of positivity constraints on $\pi\pi$ scattering amplitudes (e.g., see Refs. [14–18]). Pion–nucleon scattering was also studied in Ref. [19], in terms of the pion energy E_π in the center-of-mass rest-frame (CM) and positivity constraints were extracted for the second derivative of the $\pi^\pm p \to \pi^\pm p$ scattering amplitude with respect to E_π. However, only the $\pi^+ p$ forward scattering ($t = 0$) was analyzed in detail and no extra information was extracted from the $\pi^- p$ channel. Likewise, the positivity of its second derivative was only analyzed at two particular points, $E_\pi = \pm M_\pi/\sqrt{2}$ [19]. The central values from HB-χPT [20] were employed to check the obtained bounds. In this paper, the analysis is extended beyond the forward case $t = 0$ to the full upper part of the Mandelstam triangle $\mathcal{R}$ (with $t > 0$).

By applying the obtained positivity constraints to the corresponding EFT description of the amplitude one obtains restrictions on the LECs involved in the process at a given perturbative order. Thus, one may test whether the determination of the EFT parameters through phenomenological fits

[a] e-mail: juanj.sanz@uam.es
[b] e-mail: d.yao@fz-juelich.de
[c] e-mail: zhenghq@pku.edu.cn

to data fulfills the axiomatic constraints studied in this article. In many cases where the theoretical description is well under control and one has a good perturbative expansion the positivity lower bounds are well obeyed. This is for instance the case for $\pi\pi$-scattering in $SU(2)$ χPT [16]. However, the subthreshold constraints on the LECs are not trivially fulfilled in theories with a poor perturbative expansion (like e.g. the χPT stemming from integrating out the σ in the Linear σ Model when the scalar meson is too light [16]) or an incomplete theoretical description (as we will see in our πN analysis including Δ). Furthermore, we hope the lower bounds may help stabilizing the BχPT phenomenological fits to experimental data, where one has a poor convergence of the chiral expansion.

We want to remark that the axiomatic constraints derived in this article are general and may be applied to any theoretical framework. Indeed, there has recently been a renewed interest on the positivity issue. Following some modern lines, more stringent and precise upper bounds have been achieved on high-energy $\pi\pi$ cross section [21,22], with interesting applications of the Froissart-Martin upper bound to large-N_C $\pi\pi$ scattering [23,24]. Similar crossing, unitarity and analyticity considerations could be applied here to extract improved upper bounds for the high-energy πN cross section. However, for sake of clarity, we will focus in this article on the positivity lower bounds, previously referred, for the subthreshold region.

In Sect. 2 we introduce the general properties of pion–nucleon scattering. A particular combination D_α of the pion–nucleon scattering functions $A(s,t)$ and $B(s,t)$ is written down in terms of a positive-definite spectral function in Sect. 3. It is then used to extract the positivity constraints for both $\pi^\pm p \to \pi^\pm p$ scatterings in Sect. 4. Hence, compared to Ref. [19], extra information coming from the $B(s,t)$ function and $\pi^- p \to \pi^- p$ scattering is taken into consideration in the present work. Rather than taking two particular points to get two bounds, we scan the full region $\mathcal{R}$, extracting the most stringent bounds on the LECs. These are then tested in Sect. 5 by means of the recent results from relativistic BχPT using EOMS scheme [25–27].

This scheme is more convenient for our analysis than the HBχPT ones, as EOMS-BχPT possesses the correct analytic behavior in the Mandelstam triangle. The uncertainties due to the LEC errors and the impact of the Δ resonance are also analyzed in Sect. 5. The conclusions are summarized in Sect. 6 and some technical details as regards the positivity of the right-hand cut spectral function are relegated to the appendix.

2 Aspects of elastic pion–nucleon scattering

The effective Lagrangian describing the low-energy pion–nucleon scattering at $O(p^4)$ level takes the following form:

$$\mathcal{L}_{\pi N} = \bar{\Psi}\left\{ i\not{D} - m + \frac{g}{2}\not{u}\gamma_5 + \sum_{i=1}^{7} c_i\,\mathcal{O}_i^{(2)} + \sum_{j=1}^{23} d_j\,\mathcal{O}_j^{(3)} + \sum_{k=1}^{118} e_k\,\mathcal{O}_k^{(4)} \right\}\Psi + \cdots \tag{1}$$

where $\mathcal{O}_i^{(m)}$s ($m = 2, 3, 4$) are the operators of $O(p^m)$. Their explicit expressions can be found in Ref. [28] and the references therein. Here m and g denote the nucleon mass and the axial charge in the chiral limit. The coefficients c_i, d_j, e_k are LECs, given in units of GeV^{-1}, GeV^{-2}, and GeV^{-3}, respectively.

In the isospin limit, the scattering amplitude for the process of $\pi^a(q) + N(p) \to \pi^{a'}(q') + N(p')$ with isospin indices a and a' is described by $A^\pm(s,t)$, $B^\pm(s,t)$, and $D^\pm(s,t)$ according to [6,29–31]

$$T^{a'a}_{\pi N}(s,t) = \chi^\dagger_{N'}\left\{ \frac{1}{2}\{\tau_{a'},\tau_a\}T^+(s,t) + \frac{1}{2}[\tau_{a'},\tau_a]T^-(s,t)\right\}\chi_N \tag{2}$$

$$T^\pm(s,t) = \bar{u}(p')\left[A^\pm(s,t) + \frac{\not{q}' + \not{q}}{2}B^\pm(s,t)\right]u(p) = \bar{u}(p')\left[D^\pm(s,t) + \frac{[\not{q}',\not{q}]}{4m_N}B^\pm(s,t)\right]u(p) \tag{3}$$

$$D^\pm(s,t) = A^\pm(s,t) + \nu B^\pm(s,t) \tag{4}$$

here $\tau_{a'}$, τ_a are Pauli matrices, $\nu = (s-u)/4m_N$ and χ_N ($\chi_{N'}$) is the isospinor for the incoming (outgoing) nucleon. The Mandelstam variables s, t and u fulfill $s + t + u = 2m_N^2 + 2M_\pi^2$ with m_N and M_π, being the physical nucleon and pion masses, respectively. The functions $X^\pm$ with $X = \{A, B, D\}$ are the so-called isospin-even (for '+') and -odd (for '–') amplitudes, and they are related to the isospin amplitudes with definite isospin I (1/2 or 3/2) via

$$X^{1/2} = X^+ + 2X^- \qquad X^{3/2} = X^+ - X^-. \tag{5}$$

It is also convenient for later use to write down the relations among the $\pi^\pm p \to \pi^\pm p$ scattering amplitudes, isospin even/odd amplitudes and isospin amplitudes:

$$\begin{aligned} X^{\pi^+ p} &= X^{3/2} = X^+ - X^- \\ X^{\pi^- p} &= \frac{2}{3}X^{1/2} + \frac{1}{3}X^{3/2} = X^+ + X^-. \end{aligned} \tag{6}$$

The physical region for the pion–nucleon reaction corresponds to the kinematical region where the Kibble function [32] $\Phi = t\left[su - (m_N^2 - M_\pi^2)^2\right]$ is non-negative. In Fig. 1, the physical regions are depicted by light gray. The triangle in the center is given by $s,\ u \le (m_N + M_\pi)^2$ and $t < 4M_\pi^2$. It is the so-called Mandelstam triangle. The upper

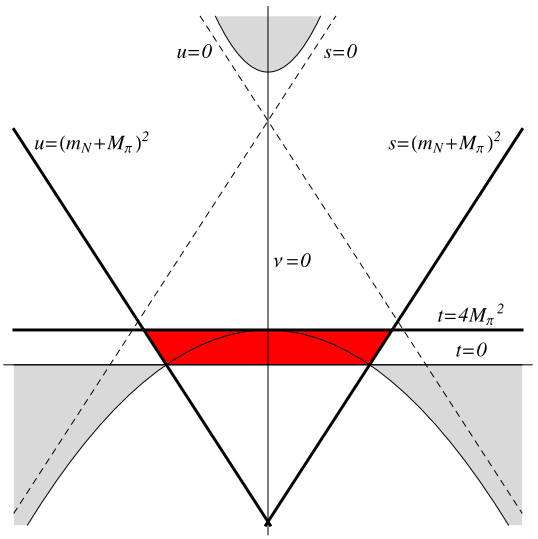

Fig. 1 Mandelstam plane (ν, t). The Mandelstam triangle is the region contoured by the $s = (m_N + M_\pi)^2$, $u = (m_N + M_\pi)^2$ and $t = 4M_\pi^2$ lines. Our region of study $\mathcal{R}$ is the trapezium formed by the three previous lines and $t = 0$, which is marked in *red*

part of the Mandelstam triangle bounded by $t \geq 0$ corresponds to the region $\mathcal{R}$ (marked in red in Fig. 1) where the positivity conditions are considered.

In terms of the (ν, t) variables the Mandelstam diagram is given by $t \leq 4M_\pi^2$ and $|\nu| \leq \nu\text{th}(t) = M_\pi + t/(4m_N)$. In order to obtain the region $\mathcal{R}$ one should add the restriction $t \geq 0$.

3 Partial-wave decomposition and positive-definite spectral function

It is well known that the full isospin amplitude can be written in terms of the partial-wave (PW) amplitudes as [33]

$$\vec{\mathcal{A}}^I(s,t)\Big|_{t=t(s,z_s)} = \sum_{\ell=0}^{\infty} S^\ell(s,z_s)\vec{\mathcal{F}}_\ell^I(s) \tag{7}$$

with

$$\vec{\mathcal{A}}^I \equiv \begin{pmatrix} A^I \\ B^I \end{pmatrix}, \quad \vec{F}_\ell^I \equiv \begin{pmatrix} f_{\ell+}^I \\ f_{(\ell+1)-}^I \end{pmatrix}$$

and

$$S^\ell(s,z_s) = 4\pi \begin{pmatrix} \left[\frac{W+m_N}{E+m_N}P'_{\ell+1}(z_s) + \frac{W-m_N}{E-m_N}P'_\ell(z_s)\right] - \left[\frac{W+m_N}{E+m_N}P'_\ell(z_s) + \frac{W-m_N}{E-m_N}P'_{\ell+1}(z_s)\right] \\ \left[\frac{1}{E+m_N}P'_{\ell+1}(z_s) - \frac{1}{E-m_N}P'_\ell(z_s)\right] - \left[\frac{1}{E+m_N}P'_\ell(z_s) - \frac{1}{E-m_N}P'_{\ell+1}(z_s)\right] \end{pmatrix}, \quad W = \sqrt{s}. \tag{8}$$

Here $P_\ell(z_s)$ are the conventional Legendre polynomials and $z_s = 1 + \frac{2s\,t}{\lambda(s,m_N^2,M_\pi^2)}$ with $\lambda(s,m_N^2,M_\pi^2) = [s-(m_N+M_\pi)^2][s-(m_N-M_\pi)^2]$, is the Källén function. The kernel matrices of this set, $S^\ell(s,z_s)$, are always analytical functions, real for real values of the Mandelstam variables (s,t,u). Thus, in the case $s \geq s_{\text{th}}$ the whole analytic discontinuity is due to the partial waves $f_k^I(s)$:

$$\text{Im}\vec{\mathcal{A}}^I(s+i\epsilon,t) = \sum_{\ell=0}^{\infty} S^\ell(s,z_s(s,t))\,\text{Im}\vec{\mathcal{F}}_\ell^I(s+i\epsilon). \tag{9}$$

Since a fixed-t dispersion relation for the analysis of the subthreshold amplitude will be used in Sect. 4, our interest is focused on obtaining a positive-definite spectral function in the physical region $s \geq s_{\text{th}}$. On the right-hand side of Eq. (9), the imaginary part of each PW is positive due to unitarity, i.e., $\text{Im}\,f_k^I(s) \geq 0$ for $s \geq s_{\text{th}}$, but the kernel matrices always contain negative elements. Therefore, it is proper to construct a combination of A^I and B^I in the form

$$\begin{aligned} D_\alpha^I(s,t) &\equiv \alpha A^I(s,t) + \nu B^I(s,t) = \alpha D^I(s,t) \\ &\quad + (1-\alpha)\nu B^I(s,t) \end{aligned} \tag{10}$$

such that its imaginary part satisfies

$$\text{Im}D_\alpha^I(s,t) \geq 0. \tag{11}$$

In order to guarantee Eq. (11), it is proven in great detail in Appendix that the validity region for the combination factor α should be $\alpha_{\min}(t) \leq \alpha \leq \alpha_{\max}(t)$ with

$$\begin{aligned} \alpha_{\min}(t) &= \frac{\left(1+\frac{t}{4m_N M_\pi}\right)\left(1-\frac{t}{4m_N^2}\right)}{\left(1+\frac{t}{2m_N M_\pi}+\frac{t}{4m_N^2}\right)} \\ &= 1 - \frac{t}{4m_N M_\pi} + \mathcal{O}\left(\frac{p^2}{m_N^2}\right), \\ \alpha_{\max}(t) &= 1 + \frac{t}{4m_N M_\pi}, \end{aligned} \tag{12}$$

where $M_\pi = \mathcal{O}(p)$ and $t = \mathcal{O}(p^2)$ [25–27].

It is worth noting that here the Mandelstam variable t must be greater than zero, $t \geq 0$, due to the application of Eq. (56) and the fact of $P'_k(z_s) \geq 0$ for $z_s \geq 1$ in the appendix. This is the reason why our analysis of the positivity constraints is restricted to the upper part of the Mandelstam triangle $\mathcal{R}$ (see Fig 1).

So far, the s-channel positive-definite spectral function above threshold is clear. The corresponding u-channel one is easily obtained by crossing symmetry:

$$D^I_\alpha(u,t) = C^{II'}_{\rm LR} D^{I'}_\alpha(s,t),$$
$$\text{(or, equivalently, } D^I_\alpha(-\nu,t) = C^{II'}_{\rm LR} D^{I'}_\alpha(\nu,t)) \tag{13}$$

with the crossing matrix being

$$C_{\rm LR} = \frac{1}{3}\begin{pmatrix} -1 & 4 \\ 2 & 1 \end{pmatrix}, \quad C^{II'}_{\rm LR} C^{I'J}_{\rm LR} = \delta_{IJ}. \tag{14}$$

where the first (second) row and column of $C_{\rm LR}$ correspond to isospin $\frac{1}{2}$ (isospin $\frac{3}{2}$). $C_{\rm LR}$ may also be found to be denoted in the bibliography as C_u.

4 Theoretical constraints indicated by the dispersion relation

For $0 \le t \le 4M_\pi^2$ it is possible to write down a fixed-t dispersion relation for $X(\nu,t)$ in terms of the ν variable (or s, if desired). If $\nu D^I_\alpha(\nu,t)$ vanished for $|\nu| \to \infty$, the amplitude $D^I_\alpha(\nu,t)$ could be represented by the unsubtracted dispersive integral,

$$D^I_\alpha(\nu,t) = \frac{Z^I_{N,R}(t)}{\nu_B - \nu} + \frac{Z^I_{N,L}(t)}{\nu_B + \nu} + \frac{1}{\pi}\int_{\nu_{\rm th}}^{\infty} {\rm d}\nu' \left[\frac{{\rm Im}D^I_\alpha(\nu'+i\epsilon,t)}{\nu'-\nu} + \frac{{\rm Im}D^I_\alpha(-\nu'-i\epsilon,t)}{\nu'+\nu}\right], \tag{15}$$

where $\nu_B(t) = \nu|_{s=m_N^2} = (t-2M_\pi^2)/(4m_N)$ and $Z^I_{N,R}(t)$ and $Z^I_{N,L}(t)$ are the residues of the s- and u-channel nucleon poles, respectively. The first term within the integral comes from the discontinuity across the right-hand cut, and the second one from the discontinuity across the left-hand cut. Since the left-hand cut spectral function ${\rm Im}D^I_\alpha(-\nu'-i\epsilon,t)$ with isospin I and the right-hand spectral function ${\rm Im}D^{I'}_\alpha(\nu'+i\epsilon,t)$ with isospin I' are related by the crossing relation in Eq. (13), the dispersion relation (15) can be rewritten as

$$\tilde{D}^I_\alpha(\nu,t) = \frac{1}{\pi}\int_{\nu_{\rm th}}^{\infty} {\rm d}\nu' \left[\frac{\delta^{II'}}{\nu'-\nu} + \frac{C^{II'}_{\rm LR}}{\nu'+\nu}\right] {\rm Im}D^{I'}_\alpha(\nu'+i\epsilon,t), \tag{16}$$

with the nucleon pole subtracted amplitude

$$\tilde{D}^I_\alpha(\nu,t) \equiv D^I_\alpha(\nu,t) - \left[\frac{Z^I_{N,R}(t)}{\nu_B-\nu} + \frac{Z^I_{N,L}(t)}{\nu_B+\nu}\right]. \tag{17}$$

In the physical case, however, $\nu D_\alpha(\nu,t)$ does not vanish at high energies and the unsubtracted dispersive integral in Eq. (16) does not converge. Nonetheless, this can easily be cured by considering a number of $n \ge 2$ of subtractions. An equivalent alternative is to take the nth derivative with respect to ν on both sides of Eq. (16) [33–35]:

$$\frac{d^n}{{\rm d}\nu^n}\tilde{D}^I_\alpha(\nu,t) = \frac{n!}{\pi}\int_{\nu_{\rm th}}^{\infty} {\rm d}\nu' \left[\frac{\delta^{II'}}{(\nu'-\nu)^{n+1}} + (-1)^n \frac{C^{II'}_{\rm LR}}{(\nu'+\nu)^{n+1}}\right] {\rm Im}D^{I'}_\alpha(\nu'+i\epsilon,t), \tag{18}$$

which is now convergent for $n \ge 2$. An analogous expression is given for the $\pi\pi$-scattering amplitude in Ref. [16].

On the right-hand cut ($\nu > \nu_{\rm th}$), the spectral functions ${\rm Im}D^{I'}_\alpha(\nu'+i\epsilon,t)$ are positive for α in the range

$$\alpha_{\rm min}(t) \le \alpha \le \alpha_{\rm max}(t). \tag{19}$$

Both denominators within the bracket in Eq. (18) happen to be positive for $\nu' \ge \nu_{\rm th}$ when $|\nu| \le \nu_{\rm th}$. If n is an even number, the relative sign is also positive. However, the factor $C^{II'}_{\rm LR}$ is negative when $I = I' = 1/2$. The aim, therefore, is to construct combinations of the isospin amplitudes in the form

$$\sum_I \beta_I \tilde{D}^I_\alpha = \beta_{1/2}\tilde{D}^{1/2}_\alpha + \beta_{3/2}\tilde{D}^{3/2}_\alpha \tag{20}$$

such that both their right- and left-cut contributions are positive definite. The inspection of Eq. (18) implies the constraints

$$\sum_I \beta_I \delta^{II'} \ge 0, \qquad \sum_I \beta_I C^{II'}_{LR} \ge 0, \tag{21}$$

which lead to

$$2\beta_{3/2} \ge \beta_{1/2} \ge 0. \tag{22}$$

As pointed out by Ref. [19], it is only necessary to investigate two cases: $\tilde{D}^{3/2}_\alpha$ and $(2\tilde{D}^{1/2}_\alpha + \tilde{D}^{3/2}_\alpha)/3$. In view of Eq. (6), these cases correspond to the physical processes $\pi^+ p \to \pi^+ p$ and $\pi^- p \to \pi^- p$, respectively. Hence, two positivity constraints on the pion–nucleon scattering amplitudes are obtained:

$$\frac{{\rm d}^n \tilde{D}^{\pi^\pm p}_\alpha(\nu,t)}{{\rm d}\nu^n} = \frac{{\rm d}^n}{{\rm d}\nu^n}\left[\tilde{D}^+_\alpha(\nu,t) \mp \tilde{D}^-_\alpha(\nu,t)\right] \ge 0 \quad \text{(for even } n\text{)}. \tag{23}$$

The forward-scattering constraints were extracted in Ref. [19] in terms of the kinematical variable s (and later reexpressed in terms of the pion energy $\omega = (s - m_N^2 + M_\pi^2)/(2\sqrt{s})$ in the center-of-mass rest-frame). They can be easily related to those in Eq. (23) by means of the relation $(2m_N)^n \frac{\partial^n \tilde{D}}{\partial s^n} = \frac{\partial^n \tilde{D}_1}{\partial \nu^n}$ for $t = 0$ (which also implied $\alpha = 1$). The inequalities above in Eq. (23) are equivalent to

$$\frac{{\rm d}^n}{{\rm d}\nu^n}\tilde{D}^+_\alpha(\nu,t) - \left|\frac{{\rm d}^n}{{\rm d}\nu^n}\tilde{D}^-_\alpha(\nu,t)\right| \ge 0, \qquad (\nu,t) \in \mathcal{R} \quad \text{(for even } n\text{)}, \tag{24}$$

and $\alpha_{\min}(t) \leq \alpha \leq \alpha_{\max}(t)$. From now on we will focus just on the $n = 2$ case, and for later convenience we will define the quantity

$$f(\alpha, \nu, t) = F_\pi^2 \frac{\mathrm{d}^2}{\mathrm{d}\nu^2} \tilde{D}_\alpha^+(\nu, t) - F_\pi^2 \left| \frac{\mathrm{d}^2}{\mathrm{d}\nu^2} \tilde{D}_\alpha^-(\nu, t) \right| \quad (25)$$

which must be positive for $(\nu, t) \in \mathcal{R}$ and $\alpha_{\min}(t) \leq \alpha \leq \alpha_{\max}(t)$.

Notice that $t = 0$ corresponds to the forward-scattering case where $\alpha = \alpha_{\min}(0) = \alpha_{\max}(0) = 1$ and $\tilde{D}_1(\nu, t) = \tilde{D}(\nu, t)$.

This case was considered in Ref. [19] within the HB-χPT framework, where, in addition, only the points with $t = 0$ and CM pion energy $\omega = \pm M_\pi/\sqrt{2}$ were analyzed. In terms of the kinematical variables considered here these correspond to the points $\frac{\nu}{M_\pi} = -\frac{M_\pi}{2m_N} \pm \frac{1}{2}\sqrt{2 - \frac{M_\pi^2}{m_N^2}} \simeq -0.07 \pm 0.70$.

In the present work, the analysis has been extended to the much wider region $\mathcal{R}$ in order to obtain more stringent positivity constraints. Moreover, the recent covariant EOMS-BχPT results [25–27] are adopted to test the resultant bounds on the LECs.

5 Numerical analysis of the positivity constraints within EOMS-BχPT

The positivity conditions on the pion–nucleon scattering amplitude, shown in Eq. (24), can be transformed into bounds on the LECs. By considering the fit results from BχPT one can test whether the bounds are respected or not at a given chiral order. However, as mentioned in Ref. [19], the scattering amplitudes within HBχPT manifest an incorrect analytic behavior inside the Mandelstam triangle, e.g., a modification of the nucleon pole structure, which causes problems with the convergence of chiral expansion. Hence, it is convenient to adopt the recent relativistic results from the EOMS-BχPT framework, employed in Refs. [25] (up to $O(p^3)$) and [26,27] (up to $O(p^4)$). In what follows, the case $n = 2$ given by Eq. (25) is chosen to derive bounds on the LECs up to $O(p^4)$ level. Thanks to a numerical analysis, we extract the most stringent bound in the region $\mathcal{R}$. We have adopted the input values $m_N = 0.939$ GeV, $M_\pi = 0.139$ GeV, $g_A = 1.267$, and $F_\pi = 0.0924$ GeV, the same as in [26,27].

The leading $O(p)$ pion–nucleon scattering amplitude is linear in ν and hence vanishes when performing the second derivatives. Up to $O(p^2)$, Eq. (25) gives for c_2 the bound

$$f(\alpha, \nu, t) = 4\alpha\, c_2 \geq 0. \quad (26)$$

Since $0.85 \leq \alpha_{\min}(t) \leq \alpha \leq \alpha_{\max}(t)$ for $0 \leq t \leq 4M_\pi^2$, the above inequality is simplified to $c_2 \geq 0$. It is trivial and well satisfied by the fit values $c_2 = 3.74 \pm 0.09\ \mathrm{GeV}^{-1}$ from Ref. [25] and $c_2 = 4.01 \pm 0.09\ \mathrm{GeV}^{-1}$ from Refs. [26,27] (see Table 1).

5.1 Analysis at $O(p^3)$ level

The scattering amplitudes in EOMS-BχPT were independently computed up to $O(p^3)$ in Refs. [25–27]. Therein, the amplitudes were employed to perform fits to existing experimental phase-shift data, determining the LECs concerned. Here, the positivity constraints, displayed by Eq. (24), provide additional information as regards the amplitudes. When $n = 2$, they turn into Eq. (25) and give bounds on the LECs at the $O(p^3)$ level:

$$f(\alpha, \nu, t) = 4\alpha c_2 - 8(\alpha - 1) m_N (d_{14} - d_{15}) - h_+^{(2)}(\alpha, \nu, t) - \left| 24\alpha\nu d_3 - h_-^{(2)}(\alpha, \nu, t) \right| \geq 0 \quad (\nu, t) \in \mathcal{R}, \quad (27)$$

with $\alpha_{\min}(t) \leq \alpha \leq \alpha_{\max}(t)$ and the second derivatives of the non-pole loop contributions,

$$h_\pm^{(2)}(\alpha, \nu, t) = -F_\pi^2 \frac{\mathrm{d}^2 \tilde{D}_\alpha^{\pm,\mathrm{loop}}(\nu, t)}{\mathrm{d}\nu^2}. \quad (28)$$

Note that the left-hand side of Eq. (27) is a multivariate function with respect to α, ν and t.

The inequality given by Eq. (27) is useful for judging the goodness of the fit results in Refs. [25–27]. In both of them the minimal value of $f(\alpha, \nu, t)$ is always achieved for $\alpha = \alpha_{\min}(t)$. After setting $\alpha = \alpha_{\min}(t)$, the scanning of (ν, t) within the region $\mathcal{R}$ yields the most stringent bound for $\nu = \pm 0.68 M_\pi$, $t = 4M_\pi^2$ in the $\mathcal{O}(p^3)$ analysis [26,27], which is well respected: $f(\alpha_{\min}(4M_\pi^2), \pm 0.68 M_\pi, 4M_\pi^2) = 0.83 \geq 0$.

In a similar way, the $\mathcal{O}(p^3)$ analysis [25] produces its most stringent bound for $\nu = \pm 0.65 M_\pi$, $t = 4M_\pi^2$ and $\alpha = \alpha_{\min}(4M_\pi^2)$, which is well fulfilled: $f(\alpha_{\min}(4M_\pi^2), \pm 0.65 M_\pi, 4M_\pi^2) = 1.03 \geq 0$.

Note that the fit results from Refs. [25–27] differ from each other slightly, leading to different positions for the minimum of $f(\alpha, \nu, t)$. This is due to fact that, although the structure of the amplitudes in these two papers is the same, the coefficients of the polynomials in the amplitudes (i.e., the tree-level ones) are different.

The contour plot for $f(\alpha, \nu, t)$ in the region $\mathcal{R}$, with $\alpha = \alpha_{\min}(t)$, is shown in Fig. 2. We used the LEC central values from Refs. [26,27]. We noticed that at $\mathcal{O}(p^3)$ the EOMS-scheme renormalized loop contributions were numerically relevant. If only the tree diagrams were considered in the inequality (25) the corresponding bound fails in some regions of $\mathcal{R}$, where $f(\alpha, \nu, t) < 0$ (see the left-hand side graph in Fig. 2). Hence, the loop contribution is crucial. It is needed

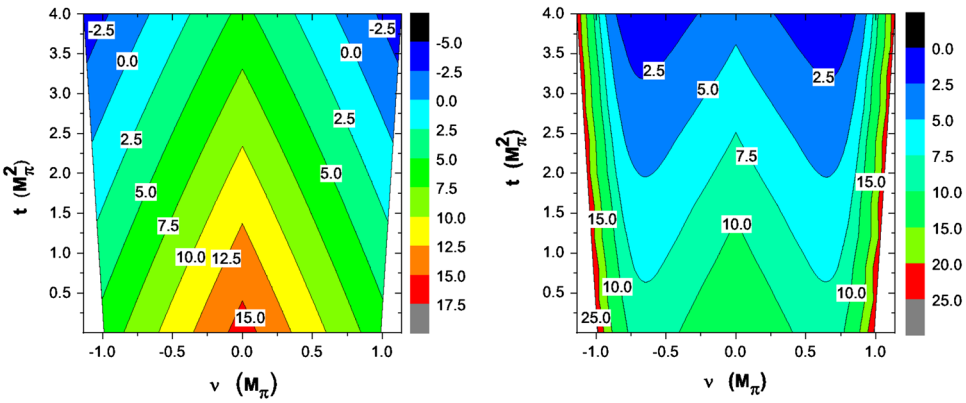

Fig. 2 Positivity bound on LECs at $O(p^3)$ level. The fit results from 'Fit I-$O(p^3)$' given in Refs. [26,27] are employed for plotting $f(\alpha, \nu, t)$ at $\mathcal{O}(p^3)$. *Left-hand side* only tree level; *right-hand-side* tree level + loops. Similar results are obtained if one uses instead the 'WI08' results with $\not\Delta$-ChPT given in Ref. [25]

Table 1 LECs involved in the positivity bounds without explicit $\Delta(1232)$ contributions. Actually, c_i in the fit I(a)-$O(p^4)$ [26,27] stand for $\hat{c}_i$. The * denotes an input quantity. c_i, d_j, and e_k have units of GeV^{-1}, GeV^{-2} and GeV^{-3}, respectively

LEC	Fit I-$O(p^3)$ [26,27]	WI08 ($\not\Delta$-ChPT) [25]	Fit I(a)-$O(p^4)$ [26,27]	Fit I(b)-$O(p^4)$ [26,27]	Fit I(c)-$O(p^4)$ [26,27]
c_1	-1.39 ± 0.07	-1.50 ± 0.06	-1.08 ± 0.06	-1.39^*	-1.09 ± 0.08
c_2	4.01 ± 0.09	3.74 ± 0.09	2.78 ± 0.11	4.01^*	2.24 ± 0.05
c_3	-6.61 ± 0.08	-6.63 ± 0.08	-5.26 ± 0.14	-6.61^*	-5.05 ± 0.22
c_4	3.92 ± 0.04	3.68 ± 0.05	2.43 ± 0.19	3.92^*	2.43 ± 0.19
d_3	-3.02 ± 0.51	-2.63 ± 0.51	-6.87 ± 0.16	-8.04 ± 0.13	-6.87 ± 0.15
$d_{14} - d_{15}$	-7.15 ± 1.06	-6.80 ± 1.07	-12.09 ± 0.24	-13.90 ± 0.20	-11.94 ± 0.23
e_{15}	–	–	-14.99 ± 0.55	-14.50 ± 0.55	-5.41 ± 0.57
e_{16}	–	–	7.35 ± 0.35	7.65 ± 0.35	4.34 ± 0.28
e_{18}	–	–	6.07 ± 1.18	-0.79 ± 1.19	6.00 ± 1.26
$e_{20} + e_{35}$	–	–	–	-12.86 ± 0.83	–
$e_{22} - 4e_{38}$	–	–	–	-8.19 ± 1.79	–

not only at the formal level for the consistence of the effective theory but also for the numerical fulfillment of the positivity constraints at this chiral order.

The analyses above were carried out with the central values of the LECs. In order to study the influence of the error and to provide a convenient inequality that can be used in future analysis, we take the particular point $\nu = \pm 0.68 M_\pi$, $t = 4M_\pi^2$, $\alpha = \alpha_{\min}(4M_\pi^2) = 0.85$, where the bound reads

$$f(\alpha, \nu, t) = 3.40 c_2 + 1.11(d_{14} - d_{15}) - 0.29 - |1.93 d_3 + 1.22| \geq 0 \quad (\nu = \pm 0.68 M_\pi,\ t = 4M_\pi^2,\ \alpha = 0.85), \tag{29}$$

with c_2 and d_j given in GeV^{-1} and GeV^{-2} units, respectively.

Contrary to what happens with the tree-level contributions to $f(\alpha, \nu, t)$, which are given by a simple polynomial of α, ν and t, the one-loop parts have a very complicated functional form and the full $f(\alpha, \nu, t)$ cannot be minimized analytically. The loop contributions can only be treated numerically—in a similar way to Ref. [17]—, yielding the contributions (-0.29) and $(+1.22)$ in Eq. (29).

Notice that the numerical coefficients in this equation do not depend on $\mathcal{O}(p^2)$ or $\mathcal{O}(p^3)$ LECs, and they are fully determined by m_N, M_π, g_A and F_π. Equation (29) provides the optimal bound for Refs. [26,27] and nearly the optimal bound for Ref. [25].

Considering now the $\mathcal{O}(p^2)$ and $\mathcal{O}(p^3)$ LEC uncertainties in the previous $\mathcal{O}(p^3)$ inequality, one gets (in units of GeV^{-1})

$$f(\alpha, \nu, t) = 5.42 \pm 1.22 - |-4.59 \pm 0.98| \stackrel{?}{\geq} 0 \quad \text{(Ref. [18])}, \tag{30}$$

$$f(\alpha, \nu, t) = 4.89 \pm 1.23 - |-3.84 \pm 0.98| \stackrel{?}{\geq} 0 \quad \text{(Ref. [17])}. \tag{31}$$

By the symbol $\stackrel{?}{\geq}$ we mean that, although we find $f(\alpha, \nu, t) \geq 0$ for the $\mathcal{O}(p^3)$-fit central values, this is not true for all the possible LEC values in the 1σ confidence region.

In Table 1 one finds details of the LECs [25–27]. Here the formula $\Delta f = \sqrt{\sum_i [f'(\overline{x}_i)\Delta x_i]^2}$ is adopted to propagate the errors of the LECs, where x_i stands for the LECs with $\overline{x}_i$ the central values and Δx_i the corresponding errors. These expressions show a violation of the positivity constraints in

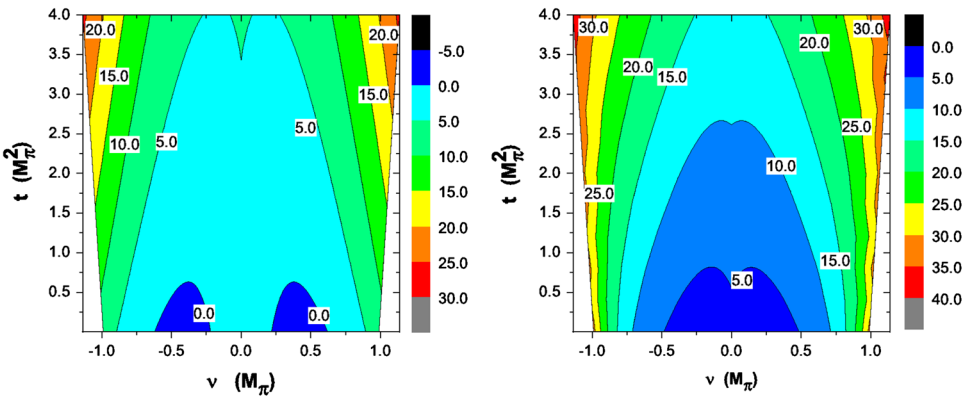

Fig. 3 Positivity bound on LECs at $O(p^4)$ level. The fit results from 'Fit I(a)-$O(p^4)$' given in Refs. [26,27] are employed for plotting $f(\alpha, \nu, t)$ up to $\mathcal{O}(p^4)$ in EOMS-BχPT. *Left-hand side* only tree level; *right-hand side* tree+loop

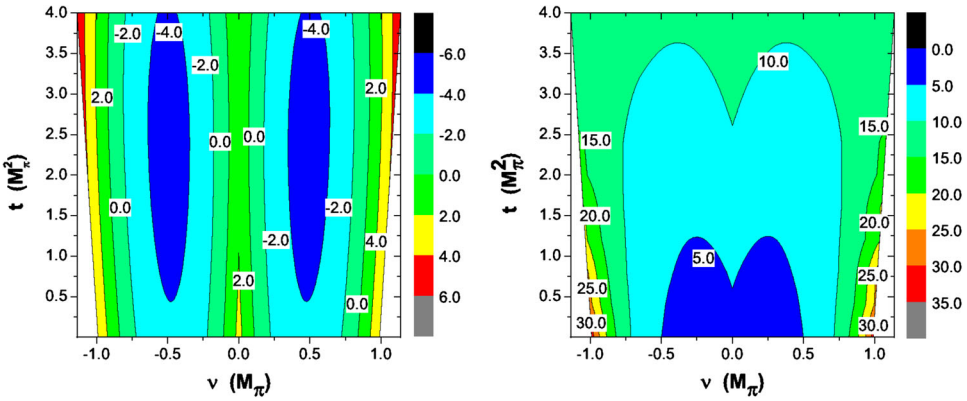

Fig. 4 Positivity bound on LECs at $O(p^4)$ level. The fit results from 'Fit I(b)-$O(p^4)$' given in Refs. [26,27] are employed for plotting $f(\alpha, \nu, t)$ up to $\mathcal{O}(p^4)$ in EOMS-BχPT. *Left-hand side* only tree level; *right-hand side* tree+loop

part of the confidence region and queries the convergence of the pion–nucleon scattering amplitude at the $O(p^3)$ level. Actually, this was first pointed out by Ref. [25] where it was argued that the pion–nucleon calculation in the EOMS scheme may have problems with the convergence of the chiral expansion. This is partly confirmed by the $\mathcal{O}(p^3)$ positivity analysis shown here, where not all the values within the 1σ confidence intervals fulfill the bound.

Thus, the constraint (29) may help to stabilize future fits to the data and the chiral expansion.

5.2 Analysis at $O(p^4)$ level

At the $O(p^4)$ level, with two subtractions ($n = 2$), the bound (25) on the LECs turns into

$$f(\alpha,\nu,t) = 4\alpha\hat{c}_2 - 8(\alpha-1)m_N(d_{14}-d_{15}) + 32\alpha\left[-\hat{c}_1\hat{c}_2M_\pi^2 - 2e_{15}m_N\nu_B + 6e_{16}\nu^2\right] - h_+^{(2)}(\alpha,\nu,t) - \left|24\alpha\nu d_3 - 96(\alpha-1)e_{18}m_N\nu - h_-^{(2)}(\alpha,\nu,t)\right| \geq 0, \quad (32)$$

where $\hat{c}_1 = c_1 - 2M_\pi^2(e_{22}-4e_{38})$ and $\hat{c}_2 = c_2 + 8M_\pi^2(e_{20}+e_{35})$ [26,27]. Here the non-pole loop terms $h_\pm^{(2)}(\alpha,\nu,t)$ contain both $O(p^3)$ and $O(p^4)$ contributions. It is useful to reexpress the bound (32) up to $\mathcal{O}(p^4)$ as

$$f(\alpha,\nu,t) = 4\alpha c_2 - 8(\alpha-1)m_N(d_{14}-d_{15}) + 32\alpha\left[(e_{20}+e_{35}-c_1c_2)M_\pi^2 - 2e_{15}m_N\nu_B + 6e_{16}\nu^2\right] - h_+^{(2)}(\alpha,\nu,t) - \left|24\alpha\nu d_3 - 96(\alpha-1)e_{18}m_N\nu - h_-^{(2)}(\alpha,\nu,t)\right| \geq 0. \quad (33)$$

These two equations differ from each other by terms of $\mathcal{O}(p^5)$ in the chiral expansion or higher.

Two different strategies were adopted in Refs. [26,27] to perform fits to the pion–nucleon phase-shift and to determine the various LECs at $O(p^4)$ level within EOMS-BχPT. The strategy called 'Fit I(a)-$O(p^4)$' provides values for the LECs in Eq. (32), and the other one, called 'Fit I(b)- $O(p^4)$', gives values for the LECs in Eq. (33).

As it happened before at $\mathcal{O}(p^3)$, the function $f(\alpha,\nu,t)$ up to $\mathcal{O}(p^4)$ also achieves its minimal values for $\alpha = \alpha_{\min}(t)$. For the central values of the LECs (see Table 1), the $\mathcal{O}(p^4)$ contour plot for $f(\alpha,\nu,t)$ in the region $\mathcal{R}$, with $\alpha = \alpha_{\min}(t)$, are shown in Figs. 3 and 4. These two figures correspond to the two different $\mathcal{O}(p^4)$ analysis, 'Fit I(a)-$\mathcal{O}(p^4)$' [26,27] in Eq. (32) and 'Fit I(b)-$\mathcal{O}(p^4)$' [26,27] in Eq. (33), respectively. The most stringent bound stemming from Eq. (32) takes the form

$$f(\alpha,\nu,t) = 4.36\hat{c}_2 - 2.74 - 0.23\hat{c}_1 - 0.23\hat{c}_3 + 0.14\hat{c}_4 + 0.11e_{16} + 0.62(e_{15} - \hat{c}_1\hat{c}_2)$$

$$
\begin{aligned}
&- |0.18 - 0.26\hat{c}_1 - 0.07\hat{c}_2 - 0.24\hat{c}_3 + 0.20\hat{c}_4 \\
&+ 0.57 d_3| \geq \quad 0, \\
&(\nu = \pm 0.17 M_\pi,\ t = 0,\ \alpha = \alpha_{\min}), \qquad (34)
\end{aligned}
$$

with c_i, d_j, and e_k in units of GeV^{-1}, GeV^{-2} and GeV^{-3}, respectively. Substituting the LECs in Eq. (34) with the values from 'Fit I(a)-$O(p^4)$' [26,27] (see Table 1), one finds (in units of GeV^{-1})

$$
f(\alpha, \nu, t) = 4.56 \pm 0.66 - |-1.88 \pm 0.11| \geq 0, \qquad (35)
$$

where the positivity constraint is definitely well obeyed at the $O(p^4)$ level in the chiral expansion.

In the alternative $\mathcal{O}(p^4)$ form (33) the most stringent bound reads

$$
\begin{aligned}
f(\alpha, \nu, t) = {} & 4.36 c_2 - 2.72 - 0.23 c_1 - 0.23 c_3 + 0.14 c_4 \\
&+ 0.11 e_{16} + 0.62(e_{15} + e_{20} + e_{35} - c_1 c_2) \\
&- |0.19 - 0.27 c_1 - 0.08 c_2 - 0.26 c_3 \\
&+ 0.21 c_4 + 0.60 d_3| \geq 0, \\
&(\nu = \pm 0.18 M_\pi,\ t = 0,\ \alpha = \alpha_{\min}), \qquad (36)
\end{aligned}
$$

with c_i, d_j, and e_k in units of GeV^{-1}, GeV^{-2} and GeV^{-3}, respectively. Substituting the values from 'Fit I(b)-$O(p^4)$' [26,27] in Table 1, we find that the positivity bound is again well respected at $O(p^4)$:

$$
f(\alpha, \nu, t) = 4.61 \pm 0.62 - |-2.04 \pm 0.08| \geq 0, \qquad (37)
$$

given in units of GeV^{-1}.

As happened at $\mathcal{O}(p^3)$, our $\mathcal{O}(p^4)$ analyses in Figs. 3 and 4 (left-hand side) show that in the EOMS scheme the bounds are violated in some regions of $\mathcal{R}$ if only the (renormalized) tree-level amplitude is included; loops play an important role, both at $O(p^3)$ and at $O(p^4)$.

5.3 Comparison at special subthreshold points

At the subthreshold region, some famous low-energy theorems can be established at particular points: the Cheng–Dashen (CD) point ($\nu = 0$, $t = 2M_\pi^2$) [36] and the Adler point ($\nu = 0$, $t = M_\pi^2$) [37,38]. The positivity bound is found to be very clearly obeyed at these points, both at $O(p^3)$ and at $O(p^4)$ (see Figs. 2, 3, and 4). Nonetheless, it is still interesting to study the evolution of the constraints at these points as the chiral order increases from $O(p^3)$ to $O(p^4)$. A priori, the variation of the bounds at the CD and Adler points should not be too large, since the chiral convergence of the amplitudes is expected to be good ($\nu \ll m_N$ and $t \ll m_N^2$) and these points are far away from non-analytical points. On the other hand, the bounds near threshold always get large values for $f(\alpha, \nu, t)$ and suffer a sizable variation from one chiral order to another as the derivatives of the loop amplitude may diverge at threshold. In what follows, the bounds at these special subthreshold points will be calculated with the condition $\alpha = \alpha_{\min}(t)$, where we extracted the most stringent bounds in the sections above.

At the CD point, where ($\nu = 0$, $t = 2M_\pi^2$), setting $\alpha = \alpha_{\min}(2M_\pi^2)$ the $O(p^3)$ bound (27) reads (in units of GeV^{-1})

$$
\begin{aligned}
&f(\alpha_{\min}(2M_\pi^2), 0, 2M_\pi^2)^{\mathcal{O}(p^3)} \\
&= \begin{cases} 8.7, & \text{for 'Fit I-}O(p^3)' \text{ from Ref. [18]}, \\ 7.9, & \text{for 'WI08' of } \not\Delta\text{-ChPT from Ref. [17]}, \end{cases} \qquad (38)
\end{aligned}
$$

and the $O(p^4)$ bounds (32) and (33) now become (in units of GeV^{-1})

$$
\begin{aligned}
&f(\alpha_{\min}(2M_\pi^2), 0, 2M_\pi^2)^{\mathcal{O}(p^4)} \\
&= \begin{cases} 8.5, & \text{for 'Fit I(a)-}O(p^4)' \text{ from [18]}, \\ 8.5, & \text{for 'Fit I(b)-}O(p^4)' \text{ from [18]}. \end{cases} \qquad (39)
\end{aligned}
$$

As expected, the $O(p^3)$ bounds at the CD point, located at the center of the upper part $\mathcal{R}$ of the Mandelstam triangle, suffer small variations when taking the EOMS-BχPT up to $O(p^4)$.

In a similar way, taking the optimal value $\alpha = \alpha_{\min}(M_\pi^2)$, the $O(p^3)$ bound (27) at the Adler point ($\nu = 0$, $t = M_\pi^2$) reads (in units of GeV^{-1})

$$
\begin{aligned}
&f(\alpha_{\min}(M_\pi^2), 0, M_\pi^2)^{\mathcal{O}(p^3)} \\
&= \begin{cases} 11.0, & \text{for 'Fit I-}O(p^3)' \text{ from Ref. [18]}, \\ 10.0, & \text{for 'WI08' of } \not\Delta\text{-ChPT from Ref. [17]}, \end{cases} \qquad (40)
\end{aligned}
$$

and the $O(p^4)$ bounds (32) and (33) give (in units of GeV^{-1})

$$
\begin{aligned}
&f(\alpha_{\min}(M_\pi^2), 0, M_\pi^2)^{\mathcal{O}(p^4)} \\
&= \begin{cases} 6.1, & \text{for 'Fit I(a)-}O(p^4)' \text{ from [18]}, \\ 6.0, & \text{for 'Fit I(b)-}O(p^4)' \text{ from [18]}. \end{cases} \qquad (41)
\end{aligned}
$$

Compared to the CD point, the variation of the bound at the Adler point is slightly larger, yet still rather acceptable.

5.4 Comparison with the IR scheme in BχPT

For the sake of completeness we have considered it convenient to perform one final analysis in BχPT. In this subsection we study the impact of considering the IR scheme [10,11] instead of the EOMS one employed above. In Fig. 5 we have plotted the value of $f(\alpha, \nu, t)$ at $\mathcal{O}(p^3)$ based on the IR analysis [39] (fit 'KA85-1').

At tree level (Fig. 5, left-hand side), we have found a similar structure to that obtained before for EOMS at $\mathcal{O}(p^3)$ (Fig. 2, left-hand side), with the polynomial contributions from the LECs slightly shifted due to the different choice of renormalization scheme. For the full bound including both tree and loop diagrams (Fig. 5, right-hand side), we have used the subthreshold expansion of the IR results [40], which shows a fair agreement with the full EOMS result in Fig. 2, right-hand side. They are only clearly different near

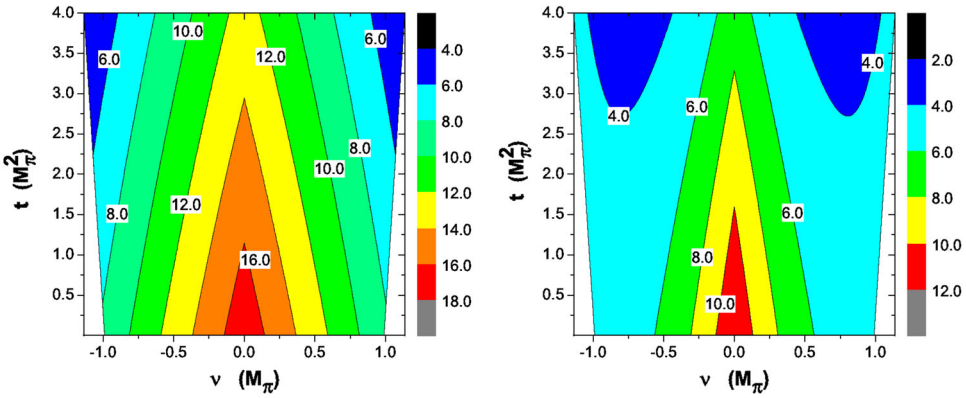

Fig. 5 The fit results from 'KA85-1' given in Ref. [39] are employed for plotting $f(\alpha, \nu, t)$ up to $\mathcal{O}(p^3)$ in IR-BχPT. *Left-hand side* only tree level; *right-hand side* tree+loop

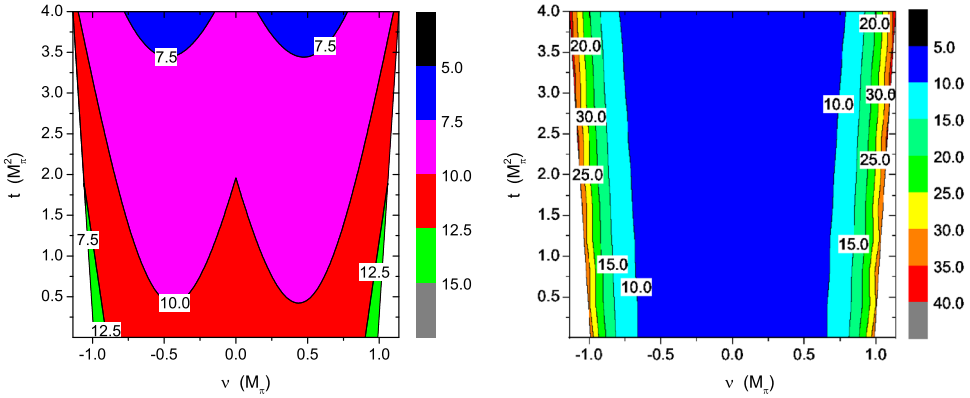

Fig. 6 Positivity bound on LECs at $O(p^3)$ level including the $\Delta(1232)$. The fit results from 'Fit II-$O(p^3)$' given in Ref. [26,27] are employed for plotting $f(\alpha, \nu, t)$. *Left-hand side* only tree level; *right-hand side* tree + loop. The analysis 'WI08' with Δ-ChPT in Ref. [25] yields a similar outcome

the threshold values $\nu = \pm\nu$th, as the subthreshold expansion employed for our IR estimate cannot reproduce the fast growing behavior of $f(\alpha, \nu, t)$ in EOMS (Fig. 2, right-hand side) due to the unexpanded one-loop logs.

Apart from this subtlety, IR BχPT seems to lead to similar results to those obtained in previous sections, at least at $\mathcal{O}(p^3)$. We find a fair agreement in spite of the various issues of the IR scheme vs. the EOMS one, such as the residual dependence of the amplitudes on the renormalization scale, the presence of an unphysical u-cut [10,11] or a large violation of the Goldberger-Treiman relation [39]. A more detailed analysis is out of the scope of the present article, where we are just presenting a novel set of axiomatic constraints.

5.5 Analysis including $\Delta(1232)$

The $\Delta(1232)$ resonance is relatively close to the πN threshold and, in particular, plays a crucial role in its P_{33} PW scattering amplitude. The absence of a large mass in the EFT is ultimately the reason why the chiral expansion here shows such a slow convergence.

The inclusion of the Δ-resonance multiplet as an explicit degree of freedom in the EFT was studied in the classic reference [41] and its contribution was explicitly included in Refs. [25–27] to describe the πN phase-shift up to center-of-mass energies of 1.20 GeV.

The corresponding LECs were pinned down through fits to the experimental data. The value of $f(\alpha, \nu, t)$ can be readily obtained from the EOMS-BχPT bounds at $\mathcal{O}(p^3)$ (Eq. (27)) and $\mathcal{O}(p^4)$ [Eqs. (32), (33)] by conveniently adding the corresponding contributions $F_\pi^2 \frac{d^2}{d\nu^2} \tilde{D}_\alpha^\pm(\nu, t)|^{\Delta-\text{Born}}$. In addition, at $\mathcal{O}(p^4)$ in the δ counting [42,43] one may have contributions from Δ resonance loops and the $\mathcal{O}(p^2)$ LECs in the one-loop diagrams need to be modified (see Appendix A.2 in Refs. [26,27]).

The contour plots for $f(\alpha, \nu, t)$ inside the upper part of the Mandelstam triangle for the $O(p^3)$ amplitude including $\Delta(1232)$ is shown in Fig. 6. Here we provided the fit results from 'Fit II-$O(p^3)$' [26,27]. The 'WI08' analysis in Ref. [25] produces similar results.

The $\mathcal{O}(p^3)$ calculations [25–27] took $\Delta(1232)$ into consideration by adding the leading Δ-Born term contribution explicitly (see the appendices therein). We find that this leading Δ-Born term provides a definite positive and large contribution to the $O(p^3)$ bounds (see Fig. 6), and both the tree-level and the full (tree+loop) bound are well obeyed.

At $O(p^4)$, the leading order Born contributions from explicit $\Delta(1232)$ exchanges were considered in Refs. [26,27] and the $\Delta(1232)$ loop contributions were also partially included. Therein, two scenarios were treated, 'Fit II(a)' and 'Fit II(b)', corresponding to the two different ways of writing down the $\mathcal{O}(p^4)$ part shown in Eqs. (32) and (33),

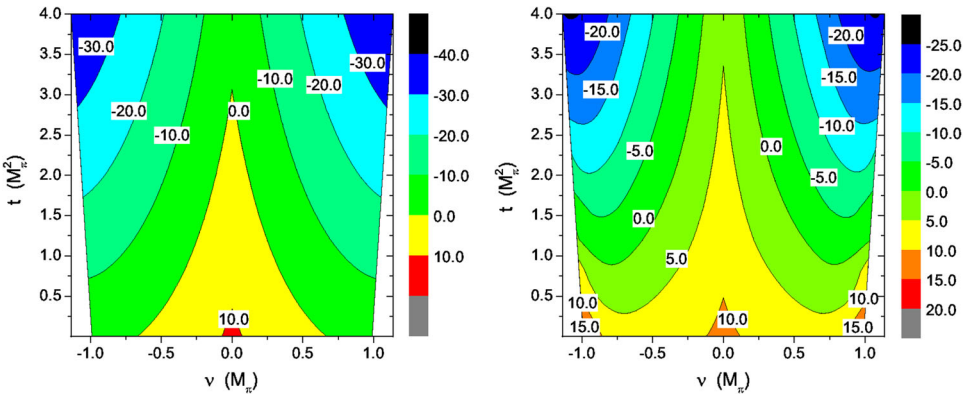

Fig. 7 Positivity bound on LECs at $O(p^4)$ level. The fit results from 'Fit II(a)-$O(p^4)$' given in Refs. [26,27] are employed for plotting $f(\alpha, \nu, t)$. *Left-hand side* only tree level; *right-hand side* tree+loop. Similar results are found with 'Fit II(b)-$O(p^4)$' from Refs. [26,27]

Table 2 LECs involved in the positivity bounds with explicit $\Delta(1232)$ contribution. The * denotes an input quantity. The c_i', d_j' and e_k' have units of GeV^{-1}, GeV^{-2} and GeV^{-3}, respectively, and h_A is dimensionless

LEC	Fit II-$O(p^3)$ [26,27]	WI08 (Δ-ChPT) [25]	Fit II(a)-$O(p^4)$ [26,27]	Fit II(b)-$O(p^4)$ [26,27]	Fit II(c)-$O(p^4)$ [26,27]
c_1'	-0.81 ± 0.03	-1.00 ± 0.04	-1.03 ± 0.03	-0.81^*	-0.95 ± 0.05
c_2'	1.46 ± 0.09	1.01 ± 0.04	0.50 ± 0.04	1.46^*	0.10 ± 0.06
c_3'	-3.10 ± 0.12	-3.04 ± 0.02	-3.17 ± 0.05	-3.10^*	-2.64 ± 0.08
c_4'	2.35 ± 0.06	2.02 ± 0.01	0.79 ± 0.03	2.35^*	0.80 ± 0.03
d_3'	-0.47 ± 0.05	-0.23 ± 0.27	-5.04 ± 0.05	-4.75 ± 0.04	-4.90 ± 0.04
$d_{14}' - d_{15}'$	-0.90 ± 0.15	-0.50 ± 0.50	-5.61 ± 0.09	-5.82 ± 0.09	-5.58 ± 0.09
e_{15}'	–	–	5.05 ± 0.13	15.29 ± 0.12	10.52 ± 0.12
e_{16}'	–	–	-0.31 ± 0.07	-2.76 ± 0.07	-1.50 ± 0.05
e_{18}'	–	–	-10.99 ± 0.12	-11.58 ± 0.11	-9.87 ± 0.12
$e_{20}' + e_{35}'$	–	–	–	-13.12 ± 0.28	–
$e_{22}' - 4e_{38}'$	–	–	–	10.29 ± 0.82	–
h_A	2.82 ± 0.04	2.87 ± 0.04	2.90^*	2.90^*	2.90^*

but now explicitly including $\Delta(1232)$. At the $\mathcal{O}(p^4)$ chiral order one needs to take into account the Δ resonance loops. Their $\mathcal{O}(p^4)$ contribution was accounted in Ref. [26,27] by adding the Δ contributions $c_1^\Delta = 0$, $c_2^\Delta = -c_3^\Delta = 2c_4^\Delta = h_A^2 m_N^2/[9m_\Delta^2(m_\Delta - m_N)]$ to the $\mathcal{O}(p^2)$ parameters c_k present in the $\mathcal{O}(p^4)$ BχPT loop.

Figure 7 shows the $f(\alpha, \nu, t)$ contour plot for 'Fit II(a)', having 'Fit II(b)' as a similar structure.

The left-hand side graph in Fig. 7 presents the contour plots if only the tree-level amplitude is taken into account, while the right-hand side shows the full bounds (tree+loop).

It is shocking that both the tree-level and full bounds are largely violated in the upper left and right corners of the region $\mathcal{R}$.

The violation of the positivity bounds implies a possible issue in the $O(p^4)$ fit results with $\Delta(1232)$ in Refs. [26,27].

To have a better understanding of this violation, one should pay attention to the unusual approach, shown in Appendix A.2 in Refs. [26,27], to include the Δ-containing loop Feynman diagrams. With this approach, the propagators of $\Delta(1232)$ occurring in the loops are integrated out, which corresponds to an expansion with respect to $1/m_\Delta$. The expansion leads to a polynomial of $1/m_\Delta$; namely, the analytic structure proportional to $\ln m_\Delta$ will never appear in the scattering amplitude. A direct and convenient way to compensate the contribution from $\ln m_\Delta$ terms is to adjust the values of the LECs of the tree amplitudes, since they are chiral polynomials. Actually, compared to the $O(p^4)$ fits without Δ, the LECs of $O(p^4)$ in fits with Δ change a lot, especially in the case of e_{18}. Moreover, the violation of the positivity bound is mainly caused by e_{18}. When the energy grows larger, bigger changes of LECs occur, possibly leading to positivity violation. Hence, the above approach of including Δ-containing loops may be practical at low energies but invalid at high energies. However, no one knows at which energy the approach fails, as the exact full expression of the Δ-containing loop amplitude is unknown. Nevertheless, the positivity bounds can tell us something. Here, the violation of the bounds shown in Fig. 7 indicates that the approach fails beyond 1.2 GeV, deserving further calculations of the exact Δ-containing loop amplitudes.

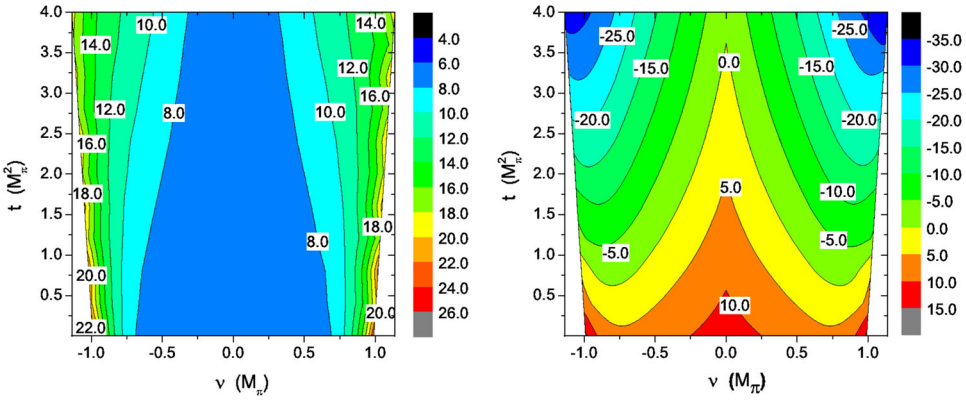

Fig. 8 Positivity bound on LECs at $O(p^4)$ level. The fit results from 'Fit I(c)-$O(p^4)$' and 'Fit II(c)-$O(p^4)$' given in Refs. [26,27] are employed for plotting $f(\alpha, \nu, t)$. *Left-hand side* full bound without explicit Δ contribution; *right-hand side* full bound with explicit Δ contribution

To conclude, at $O(p^3)$ level, both the tree-level and full bounds with Δ contribution are well satisfied, since the leading Born term of Δ gives a large and positive contribution. At $O(p^4)$ level, the bounds are badly violated, which might be mainly due to the unusual way of including the Δ-containing loop contribution. The violation indicates that a further exact and full calculation of the Δ-containing loop is necessary when performing fits beyond the energy of 1.2 GeV in the center of mass frame.

Finally, we would also like to discuss the impact of these constraints on the values of the pion–nucleon sigma term, $\sigma_{\pi N}$, analyzed in Refs. [26,27]. Therein, the lattice QCD data for m_N and the pion–nucleon scattering data were employed to determine the pion–nucleon sigma term. As a consequence, two different results were reported: $\sigma_{\pi N} = 52 \pm 7$ MeV ('Fit I(c)-$\mathcal{O}(p^4)$' without $\Delta(1232)$) and $\sigma_{\pi N} = 45 \pm 6$ MeV ('Fit II(c)-$\mathcal{O}(p^4)$' with explicit $\Delta(1232)$ contributions). However, though compatible, one may wonder which value is more accurate and carries less theoretical uncertainties.

The positivity bounds derived in this work may provide an answer to this.

The values from 'Fit I(c)-$O(p^4)$' and 'Fit II(c)-$O(p^4)$' for the LECs involved in the bounds are listed in Tables 1 and 2, respectively. The contour plots for the positivity bounds, without and with explicit Δ contribution, are shown in Fig. 8.

As we can see, the bound with Δ contribution are violated in most of the region $\mathcal{R}$, while the one without explicit Δ contribution are well satisfied. This may imply that the value $\sigma_{\pi N} = 52 \pm 7$ MeV is more reasonable than $\sigma_{\pi N} = 45 \pm 6$ MeV. Again we owe this to the lack of an exact calculation of the Δ-containing loop.

6 Conclusions

Using the general S-matrix arguments, such as analyticity, crossing symmetry and unitarity, we derived a set of positivity constraints on the pion–nucleon scattering amplitudes $D_\alpha(\nu, t) = \alpha A(\nu, t) + \nu B(\nu, t)$ in the upper part of Mandelstam triangle, $\mathcal{R}$. The outcomes and computations performed in this article can be summarized in the following points:

- We have extracted a novel generalized lower bound for πN scattering amplitudes within the subthreshold region $\mathcal{R}$, not only for forward scattering.
- The positivity lower bound has been applied to previous BχPT analyses in the EOMS scheme at $\mathcal{O}(p^3)$ and $\mathcal{O}(p^4)$, leading to optimized lower bounds on appropriate combinations LECs. The bounds have constrained the uncertainty range allowed by the phenomenological fits for the $\mathcal{O}(p^3)$ fits and we find they are fully fulfilled at $\mathcal{O}(p^4)$.
- Our general positivity constraints have also been shown for special subthreshold points (CD and Adler points).
- We have performed a first comparison of the EOMS and IR scheme, finding a fair agreement.
- We have tested how recent chiral analysis explicitly including Δ fulfills the positivity constraints, finding some issues at $\mathcal{O}(p^4)$ which call for improved computations along this line.

More in detail, these constraints were further changed into bounds on the chiral LECs of the pion–nucleon Lagrangian both at $O(p^3)$ and at $O(p^4)$ level. In combination with the central values of the LECs from Refs. [25–27] within EOMS-BχPT, it was found that the bounds at tree level are always violated in some regions inside $\mathcal{R}$, while the full bounds (tree+loop) were well respected both for $O(p^3)$ and $O(p^4)$ analyses; loops are important and, in the chosen renormalization scheme (EOMS), they produce contributions to the positivity bound numerically of the same order as the tree-level diagrams.

Nonetheless, when considering the LEC uncertainties, the full and most stringent bounds at $O(p^3)$ level are slightly violated in some parts of the 1σ intervals, pointing out the break down of EOMS-BχPT for those LEC values. However, this problem disappears as the analysis is taken up to $O(p^4)$,

where the most stringent bounds are well obeyed in the full error interval.

We have provided the constraints for special points where the bounds are nearly optimal in terms of just a few $\mathcal{O}(p^2)$, $\mathcal{O}(p^3)$, and $\mathcal{O}(p^4)$ LECs (depending on the chiral order one works at). We hope that these positivity conditions can be easily implemented and employed to constrain future BχPT analyses.

Finally, the positivity bounds with an explicit Δ resonance have been also studied. The Δ Born term provides a positive-definite contribution to the bounds and hence the bounds at $O(p^3)$ level in the δ-counting rule (see Refs. [42,43]) are well satisfied. However, at the $O(p^4)$ level, the bounds are violated when just a part of the Δ loops are included. We think that a complete one-loop calculation including Δ-loops will solve this issue.

Acknowledgments This work is supported in part by National Nature Science Foundations of China under Contract Nos. 10925522 and 11021092, the MICINN, Spain, under contract FPA2010-17747 and Consolider-Ingenio CPAN CSD2007-00042, the MICINN-INFN fund AIC-D-2011-0818, the Comunidad de Madrid through Proyecto HEP-HACOS S2009/ESP-1473 and the Spanish MINECO Centro de excelencia Severo Ochoa Program under grant SEV-2012-0249. The work of DLY was partly performed at Peking University.

Appendix: Positive-definite spectral function for D^I_α

The dispersion relation for the analysis of the subthreshold amplitude is used to extract the positivity constraints. Hence a positive-definite spectral function in the physical region $s \geq s\text{th}$ is required. Starting from Eqs. (8) and (9), one can immediately construct a preliminary combination of the form

$$0 \leq \text{Im}\left\{\alpha_1 A^I(s,t) + \alpha_2 B^I(s,t)\right\} = \vec{\alpha}^{\,T} \cdot \text{Im}\vec{\mathcal{A}}^I(s,t), \quad \text{where} \quad \vec{\alpha} = \begin{pmatrix}\alpha_1 \\ \alpha_2\end{pmatrix}. \tag{42}$$

Notice that in principle there is no restriction to the possible combinations we may consider, so one may consider combinations where $\vec{\alpha}$ depends also on s and t or, conversely, on ν and ν_B. The only necessary condition will be that they are analytical functions in the ν-integration domain in our fixed-t dispersion relation, i.e., they are real and do not contain discontinuities for $\nu \geq \nu_{\text{th}}$ for fixed t. Thus, for later convenience we will rather write the general combination of A^I and B^I in the form

$$0 \leq \text{Im}\left\{\alpha_1 A^I(s,t) + \alpha_2 \nu B^I(s,t)\right\} = \vec{\alpha}^{\,T} \cdot \text{Im}\vec{\mathcal{A}}^I(s,t), \quad \text{with } \vec{\alpha} = \begin{pmatrix}\alpha_1 \\ \alpha_2 \nu\end{pmatrix}, \tag{43}$$

where we introduced the ν factor in the $B^I(s,t)$ term. From now on we will use the notation

$$D^I_\alpha(s,t) \equiv \vec{\alpha}^{\,T} \cdot \vec{\mathcal{A}}^I(s,t). \tag{44}$$

For the study of the positivity of $\text{Im}D^I_\alpha$ we will make use of the positivity of each PW, i.e., $\text{Im}f^I_k(s) \geq 0$ for $s \geq s\text{th}$. Thus, we have

$$\begin{aligned} 0 \leq \text{Im}D^I_\alpha(s,t) &= \vec{\alpha}^{\,T} \cdot \sum_{\ell=0}^{\infty} S^\ell(s,t)\, \text{Im}\vec{\mathcal{F}}^I_\ell(s) \\ &= \sum_{\ell=0}^{\infty} \vec{\alpha}^{\,T} S^\ell(s,t)\, \text{Im}\vec{\mathcal{F}}^I_\ell(s) \\ &= \sum_{\ell=0}^{\infty} \left(\vec{\alpha}^{\,T}\vec{v}_1^{\,\ell},\ \vec{\alpha}^{\,T}\vec{v}_2^{\,\ell}\right) \text{Im}\vec{\mathcal{F}}^I_\ell(s). \end{aligned} \tag{45}$$

For convenience, here the 2×2 matrix $S^\ell(s,t)$ has been written in terms of two dimension-2 vectors:

$$S^\ell(s,z_s) = \left(\vec{v}_1^{\,\ell},\ \vec{v}_2^{\,\ell}\right). \tag{46}$$

Hence the positivity of $\text{Im}f^I_k(s)$ ensures the positivity of $\text{Im}D_\alpha(s,t)$ whenever

$$\vec{\alpha}^{\,T}\vec{v}_1^{\,\ell} \geq 0, \qquad \vec{\alpha}^{\,T}\vec{v}_2^{\,\ell} \geq 0, \tag{47}$$

for $s \geq s\text{th}$. The explicit form of these constraints is given by

$$\begin{aligned} &\frac{4\pi}{E^2 - m_N^2}\left(c_{11}(s,t)\,\alpha_1 + c_{12}(s,t)\,\nu\,\alpha_2\right) \geq 0, \\ &-\frac{4\pi}{E^2 - m_N^2}\left(c_{21}(s,t)\,\alpha_1 + c_{22}(s,t)\,\nu\,\alpha_2\right) \geq 0, \end{aligned} \tag{48}$$

with

$$\begin{aligned} c_{11} &= \frac{1}{2W}\left[(W+m_N)(W-W_+)(W-W_-)P'_{\ell+1}(z_s)\right. \\ &\quad \left. + (W-m_N)(W+W_+)(W+W_-)P'_\ell(z_s)\right], \\ c_{12} &= (E-m_N)P'_{\ell+1}(z_s) - (E+m_N)P'_\ell(z_s), \\ c_{21} &= \frac{1}{2W}\left[(W+m_N)(W-W_+)(W-W_-)P'_\ell(z_s)\right. \\ &\quad \left. + (W-m_N)(W+W_+)(W+W_-)P'_{\ell+1}(z_s)\right], \\ c_{22} &= (E-m_N)P'_\ell(z_s) - (E+m_N)P'_{\ell+1}(z_s), \end{aligned} \tag{49}$$

and the kinematical variables are

$$z_s(t,s) = 1 + \frac{t}{2\vec{q}^{\,2}}, \qquad |\vec{q}| = \sqrt{\frac{\lambda(s, M_\pi^2, m_N^2)}{4s}},$$
$$W = \sqrt{s}, \qquad E = \sqrt{\vec{q}^{\,2} + m_N^2} = \frac{W^2 + m_N^2 - M_\pi^2}{2W},$$
$$W_\pm^2 = (m_N \pm M_\pi)^2, \qquad s_{\rm th} = s_+, \tag{50}$$

with $\vec{q}$ being the three-momentum of the pion in the center-of-mass rest frame.

Since $E \geq m_N$ when $s \geq s$th we can simplify the inequalities to the form

$$c_{11}\,\alpha_1 + c_{12}\,\nu\,\alpha_2 \geq 0,$$
$$c_{21}\,\alpha_1 + c_{22}\,\nu\,\alpha_2 \leq 0. \tag{51}$$

The coefficients c_{mn} are combinations of the first derivatives of the Legendre polynomials, and in general the sign may change from one partial wave ℓ to another ℓ', or from an energy (s,t) to another. However, when $z_s(s,t) \geq 1$, i.e., when $t \geq 0$ for $s \geq s$th, one has $P_k'(z_s) \geq 0$ and then

$$c_{11} \geq 0, \qquad c_{21} \geq 0, \tag{52}$$

for any $s \geq s$th and $t \geq 0$ (as $W \geq m_N \geq 0$ and $W \geq W_\pm > 0$). Thus, the inequalities get simplified into the form

$$\alpha_1 \geq -\frac{c_{12}}{c_{11}}\,\nu\,\alpha_2, \qquad \alpha_1 \leq -\frac{c_{22}}{c_{21}}\,\nu\,\alpha_2. \tag{53}$$

One can further simplify this expression by means of the relations $(E \pm m_N) = (W \pm W_+)(W \pm W_-)/(2W)$. We can then write the inequalities in the form

$$\alpha_1 \geq -\alpha_2 \frac{\nu}{W + m_N}\left[\frac{1 - g_+^\ell(s,t)}{1 + \frac{(W-m_N)}{(W+m_N)} g_+^\ell(s,t)}\right],$$
$$\alpha_1 \leq \alpha_2 \frac{\nu}{W - m_N}\left[\frac{1 - g_-^\ell(s,t)}{1 + \frac{(W+m_N)}{(W-m_N)} g_-^\ell(s,t)}\right], \tag{54}$$

with

$$g_\pm^\ell(s,t) = \frac{(W \pm W_+)(W \pm W_-)}{(W \mp W_+)(W \mp W_-)}\,\frac{P_\ell'(z_s)}{P_{\ell+1}'(z_s)}. \tag{55}$$

Notice that these functions depend not only on the energy (s,t) but also on the PW index ℓ. Hence, we will have to obtain the region obtained by the overlap of all the PW constraints. The analysis of the Legendre polynomials tells us that for $z_s \geq 1$,

$$\frac{P_\ell'(z_s)}{P_{\ell+1}'(z_s)} < \frac{P_{\ell+1}'(z_s)}{P_{\ell+2}'(z_s)} < \lim_{\ell\to\infty} \frac{P_\ell'(z_s)}{P_{\ell+1}'(z_s)} = \frac{1}{z_s + \sqrt{z_s^2 - 1}}. \tag{56}$$

Thus, we can define the upper-bound functions for $t \geq 0$ and $s \geq s_{\rm th}$ (which implies $z_s \geq 1$),

$$\bar{g}_\pm(s,t) = \frac{(W \pm W_+)(W \pm W_-)}{(W \mp W_+)(W \mp W_-)}\left[\frac{1}{z_s + \sqrt{z_s^2 - 1}}\right] \geq g_\pm^\ell(s,t). \tag{57}$$

Hence, the intersection of all the PW's ℓ is given by the most stringent constraints for $t \geq 0$ and $s \geq s$th, given by the limit functions $\bar{g}_\pm(s,t)$:

$$\alpha_1 \geq -\alpha_2 \frac{\nu}{W + m_N}\left[\frac{1 - \bar{g}_+(s,t)}{1 + \frac{(W-m_N)}{(W+m_N)}\bar{g}_+(s,t)}\right],$$
$$\alpha_1 \leq \alpha_2 \frac{\nu}{W - m_N}\left[\frac{1 - \bar{g}_-(s,t)}{1 + \frac{(W+m_N)}{(W-m_N)}\bar{g}_-(s,t)}\right]. \tag{58}$$

These two constraints have (at least) an allowed region in the quadrant $\alpha_{1,2} \geq 0$, bounded by the two straight lines provided by these inequalities.

Now we proceed to the analysis of the bounds for the variable $s \geq s$th. One can see that the most stringent constraints come from the range where

$$-\frac{\nu}{W + m_N}\left[\frac{1 - \bar{g}_+(s,t)}{1 + \frac{(W-m_N)}{(W+m_N)}\bar{g}_+(s,t)}\right], \tag{59}$$

is maximum and where

$$\frac{\nu}{W - m_N}\left[\frac{1 - \bar{g}_-(s,t)}{1 + \frac{(W+m_N)}{(W-m_N)}\bar{g}_-(s,t)}\right] \tag{60}$$

is minimum. For fixed t one can check that the respective maximum and minimum are always found for $s = s$th. Thus, the most restricted region among all $s \geq s$th for fixed $t \geq 0$ is given by

$$\alpha_1 \geq \alpha_2\,\alpha_{\rm min}(t), \qquad \alpha_1 \leq \alpha_2\,\alpha_{\rm max}(t), \tag{61}$$

with

$$\alpha_{\rm min}(t) = \lim_{s\to s{\rm th}} (-1) \times \frac{\nu}{W + m_N}\left[\frac{1 - \bar{g}_+(s,t)}{1 + \frac{(W-m_N)}{(W+m_N)}\bar{g}_+(s,t)}\right]$$
$$= \frac{(4m_N^2 - t)(4m_N M_\pi + t)}{4m_N(4m_N^2 M_\pi + 2m_N t + M_\pi t)}$$
$$= 1 - \frac{t}{4m_N M_\pi} + \frac{t(t - 4M_\pi^2)}{8M_\pi^2 m_N^2} + \mathcal{O}\left(\frac{p^3}{m_N^3}\right),$$
$$\alpha_{\rm max}(t) = \lim_{s\to s{\rm th}} \frac{\nu}{W - m_N}\left[\frac{1 - \bar{g}_-(s,t)}{1 + \frac{(W+m_N)}{(W-m_N)}\bar{g}_-(s,t)}\right]$$
$$= 1 + \frac{t}{4m_N M_\pi}, \tag{62}$$

with $M_\pi = \mathcal{O}(p)$ and $t = \mathcal{O}(p^2)$ [26,27]. For $0 \leq t \leq 4M_\pi^2$ one has $\alpha_{\rm min}(t) \leq 1 - t/(4m_N M_\pi)$.

Taking into account that the Mandelstam triangle, free of analytical cut-singularities, is given by $s \leq (m_N + M_\pi)^2$, $u \leq (m_N + M_\pi)^2$, and $t \leq 4M_\pi^2$, in combination with our

positivity assumption $t \geq 0$, we find that only combinations with $\alpha_1 \geq 0$ and $\alpha_2 \geq 0$ are allowed; so, up to a global irrelevant positive number α_2, the constraints finally become (after relabeling α_1 as $\alpha\,\alpha_2$)

$$\alpha_{\min}(t) \leq \alpha \leq \alpha_{\max}(t). \tag{63}$$

Notice that we have optimized the bound for α for every ℓ and $s \geq s$th. Thus, finally, this condition ensures the positivity of the spectral function combination for $s \geq s$th and $t \geq 0$,

$$\mathrm{Im}D^I_\alpha(s,t) \geq 0. \tag{64}$$

The combination can then be written in the form

$$D^I_\alpha = \alpha A^I + \nu B^I = \alpha D^I + (1-\alpha)\,\nu B^I, \tag{65}$$

where $D^I_1(\nu,t)$ is equal to the usual $D^I(\nu,t)$.

References

1. S. Weinberg, Physica A **96**, 327 (1979)
2. J. Gasser, H. Leutwyler, Annals Phys. **158**, 142 (1984)
3. J. Gasser, H. Leutwyler, Nucl. Phys. B **250**, 465 (1985)
4. B.H. Bransden, R.G. Moorhouse, *The pion-nucleon system* (Princeton University Press, Princeton, 1973)
5. G. Höhler, *Landolt-Börnstein*, vol. 9b2, ed. by H. Schopper (Springer, Berlin, 1983)
6. J. Gasser, M.E. Sainio, A. Svarc, Nucl. Phys. B **307**, 779 (1988)
7. V. Bernard, Prog. Part. Nucl. Phys. **60**, 82 (2008). [arXiv:0706.0312 [hep-ph]]
8. E.E. Jenkins, A.V. Manohar, Phys. Lett. B **255**, 558 (1991)
9. V. Bernard, N. Kaiser, J. Kambor, U.G. Meissner, Nucl. Phys. B **388**, 315 (1992)
10. T. Becher, H. Leutwyler, Eur. Phys. J. C **9**, 643 (1999)
11. P.J. Ellis, H.-B. Tang, Phys. Rev. C **57**, 3356 (1998). [arXiv:hep-ph/9709354]
12. J. Gegelia, G. Japaridze, Phys. Rev. D **60**, 114038 (1999)
13. T. Fuchs, J. Gegelia, G. Japaridze, S. Scherer, Phys. Rev. D **68**, 056005 (2003)
14. B. Ananthanarayan, D. Toublan, G. Wanders, Phys. Rev. D **51**, 1093 (1995)
15. P. Dita, Phys. Rev. D **59**, 094007 (1999)
16. A.V. Manohar, V. Mateu, Phys. Rev. D **77**, 094019 (2008)
17. V. Mateu, Phys. Rev. D **77**, 094020 (2008)
18. Z.-H. Guo, O. Zhang, H.Q. Zheng, AIP Conf. Proc. **1343**, 259 (2011)
19. M. Luo, Y. Wang, G. Zhu, Phys. Lett. B **649**, 162 (2007)
20. N. Fettes, U.-G. Meissner, S. Steininger, Nucl. Phys. A **640**, 199 (1998)
21. T.T. Wu, A. Martin, S.M. Roy, V. Singh, Phys. Rev. D **84**, 025012 (2011). [arXiv:1011.1349 [hep-ph]]
22. A. Martin, S.M. Roy. [arXiv:1306.5210 [hep-ph]]
23. D. Greynat, E. de Rafael, Phys. Rev. D **88**, 034015 (2013). [arXiv:1305.7045 [hep-ph]]
24. D. Greynat, E. de Rafael, G. Vulvert. [arXiv:1312.2881 [hep-ph]]
25. J.M. Alarcon, J.M. Camalich, J.A. Oller, Annals Phys. **336**, 413 (2013)
26. Y.-H. Chen, D.-L. Yao, H. Q. Zheng. Phys. Rev. D **87**, 054019 (2013)
27. Y.-H. Chen, D.-L. Yao, H. Q. Zheng, Nucl. Phys. Proc. Suppl. **234**, 249 (2013)
28. N. Fettes, U.-G. Meissner, M. Mojzis, S. Steininger, Annals Phys. **283**, 273 (2000)
29. T. Becher, H. Leutwyler, JHEP **0106**, 017 (2001)
30. P. Buettiker, U.G. Meissner, Nucl. Phys. A **668**, 97 (2000). [arXiv:hep-ph/9908247]
31. N. Fettes, U.G. Meissner, Nucl. Phys. A **676**, 311 (2000). [arXiv:hep-ph/0002162]
32. T.W.B. Kibble, Phys. Rev. **117**, 1159 (1960)
33. C. Ditsche, M. Hoferichter, B. Kubis, U.-G. Meissner, JHEP **1206**, 043 (2012)
34. G. Hohler, in *Pion-Nucleon Scattering* Landolt-Bornstein New Series, vol. I/9b2, ed. H. Schopper (Springer, New York, 1983)
35. J. Hamilton, W.S. Woolcock, Rev. Mod. Phys. **35**, 737 (1963)
36. T.P. Cheng, R.F. Dashen, Phys. Rev. Lett. **26**, 594 (1971)
37. S.L. Adler, Phys. Rev. **137**, B1022 (1965)
38. S.L. Adler, Phys. Rev. **139**, B1638 (1965)
39. J.M. Alarcon, J. Martin Camalich, J.A. Oller. Phys. Rev. C **83**, 055205 (2011). [arXiv:1102.1537 [nucl-th]]
40. T. Becher, H. Leutwyler, JHEP **0106**, 017 (2001). [arXiv:hep-ph/0103263]
41. T.R. Hemmert, B.R. Holstein, J. Kambor, J. Phys. G **24**, 1831 (1998). [arXiv:hep-ph/9712496]
42. V. Pascalutsa, D.R. Phillips, Phys. Rev. C **67**, 055202 (2003)
43. V. Pascalutsa, M. Vanderhaeghen, S.N. Yang, Phys. Rept. **437**, 125 (2007)